Shock-synthesized hexagonal diamonds in Younger Dryas boundary sediments

Douglas J. Kennett[a,1], James P. Kennett[b], Allen West[c], G. James West[d], Ted E. Bunch[e], Brendan J. Culleton[a], Jon M. Erlandson[a,f], Shane S. Que Hee[g], John R. Johnson[h], Chris Mercer[i,j], Feng Shen[k], Marilee Sellers[e], Thomas W. Stafford, Jr.[l], Adrienne Stich[m], James C. Weaver[n], James H. Wittke[e], and Wendy S. Wolbach[m]

[a]Department of Anthropology and [f]Museum of Natural and Cultural History, University of Oregon, Eugene, OR 97403; [b]Department of Earth Science and Marine Science Institute and [j]Materials Department, University of California, Santa Barbara, CA 93106; [c]GeoScience Consulting, Dewey, AZ 86327; [d]Department of Anthropology, University of California, Davis, CA 95616; [e]Department of Geology and Imaging and Histology Core Facility, Northern Arizona University, Flagstaff, AZ 86011; [g]Department of Environmental Health Sciences, University of California, Los Angeles, CA 90095-1772; [h]Santa Barbara Museum of Natural History, 2559 Puesta del Sol, Santa Barbara, CA 93105; [i]National Institute for Materials Science, Tsukuba, Ibaraki 305-0047, Japan; [k]FEI Company, 5350 Northeast Dawson Creek Drive, Hillsboro, OR 97124; [l]Stafford Research, Inc., 200 Acadia Avenue, Lafayette, CO 80026; [m]Department of Chemistry, DePaul University, Chicago, IL 60604; and [n]Department of Chemical and Environmental Engineering, University of California, Riverside, CA 92521

Communicated by Steven M. Stanley, University of Hawaii, Honolulu, HI, June 11, 2009 (received for review March 3, 2009)

The long-standing controversy regarding the late Pleistocene megafaunal extinctions in North America has been invigorated by a hypothesis implicating a cosmic impact at the Ållerød-Younger Dryas boundary or YDB (≈12,900 ± 100 cal BP or 10,900 ± 100 ^{14}C years). Abrupt ecosystem disruption caused by this event may have triggered the megafaunal extinctions, along with reductions in other animal populations, including humans. The hypothesis remains controversial due to absence of shocked minerals, tektites, and impact craters. Here, we report the presence of shock-synthesized hexagonal nanodiamonds (lonsdaleite) in YDB sediments dating to ≈12,950 ± 50 cal BP at Arlington Canyon, Santa Rosa Island, California. Lonsdaleite is known on Earth only in meteorites and impact craters, and its presence strongly supports a cosmic impact event, further strengthened by its co-occurrence with other nanometer-sized diamond polymorphs (n-diamonds and cubics). These shock-synthesized diamonds are also associated with proxies indicating major biomass burning (charcoal, carbon spherules, and soot). This biomass burning at the Younger Dryas (YD) onset is regional in extent, based on evidence from adjacent Santa Barbara Basin and coeval with broader continent-wide biomass burning. Biomass burning also coincides with abrupt sediment mass wasting and ecological disruption and the last known occurrence of pygmy mammoths (*Mammuthus exilis*) on the Channel Islands, correlating with broader animal extinctions throughout North America. The only previously known co-occurrence of nanodiamonds, soot, and extinction is the Cretaceous-Tertiary (K/T) impact layer. These data are consistent with abrupt ecosystem change and megafaunal extinction possibly triggered by a cosmic impact over North America at ≈12,900 ± 100 cal BP.

Arlington Canyon | biomass burning | cosmic impact | hexagonal nanodiamonds | megafaunal extinctions

Thirty-five mammal and 19 bird genera became extinct in North America near the end of the Pleistocene (1, 2). Other animal populations were severely reduced or suffered massive range restrictions (3). Most of these animals were large, although smaller animals also underwent major biogeographic changes, and some also became extinct (1, 4). Detailed extinction and biogeographic histories for many of these genera are poorly known, but at least 16 genera and several additional species became extinct abruptly over broad parts of North America close to 13,000 years ago (5, 6). In situ bones of the most common large genera on the late Pleistocene landscape [e.g., *Equus* (horses), *Camelops* (camels), and *Mammuthus* (mammoths)] occur widely in North American sedimentary sequences up to, but never above, the base of a distinctive organic-rich black sedimentary layer (5). This biostratigraphic marker dates to ≈12.9 ± 0.1 ka (10,900 ± 100 ^{14}C years)* and indicates that some of the most common genera disappeared synchronously and broadly over North America.

A long-standing debate has culminated in a polarized standoff regarding the hypothesized role of climatic change versus human predation for the demise of these animals and is "further from resolution than it has been in its 200-year history (1)." The debate continues because the available empirical evidence supports neither hypothesis very well. Climatic and vegetation shifts certainly contributed to biogeographic changes in North America during the late Pleistocene, but the animal genera involved were highly adapted to frequent climatic oscillations of equal or greater magnitude during the late Quaternary (2). The absence of kill sites for most of these genera and paucity for others is also inconsistent with the alternative hypothesis; that humans rapidly drove all of these animals into extinction. Given the technology involved, along with several other significant problems (7, 8), it is highly unlikely that humans rapidly triggered the extinction of so many genera on a continental scale, although human-caused extinction is well supported in the prehistoric record of vulnerable island animal populations (e.g., 7, 9, 10). More sophisticated models combining environmental and human induced causes (e.g., 11) are potentially viable for explaining singular mammal extinctions (e.g., *Mammuthus*), but fall short of explaining the full taxonomic depth and ecological breadth of the latest Pleistocene extinctions.

This debate has recently been challenged by a hypothesis that ecosystem disruption and widespread extinctions were triggered by multiple airbursts/impacts (by comet or carbonaceous chondrite) in North America at 12.9 ± 0.1 ka (12, 13). Although controversial when first proposed, a major cosmic impact at the Cretaceous-Tertiary (K/T) boundary is now widely accepted as the cause of one of the largest known mass extinctions (14). The connection of impact-to-extinction and the presence of several of the same impact proxies in this widespread 12,900-year-old sedimentary layer provide an empirical basis for the Younger Dryas boundary (YDB) impact

Author contributions: D.J.K., J.P.K., T.E.B., J.M.E., S.S.Q.H., F.S., and W.S.W. designed research; D.J.K., J.P.K., A.W., G.J.W., T.E.B., B.J.C., J.M.E., J.R.J., C.M., F.S., M.S., A.S., J.C.W., J.H.W., and W.S.W. performed research; S.S.Q.H. and W.S.W. contributed new reagents/analytic tools; D.J.K., J.P.K., A.W., G.J.W., T.E.B., J.M.E., C.M., F.S., T.W.S., J.C.W., J.H.W., and W.S.W. analyzed data; and D.J.K. and J.P.K. wrote the paper.

The authors declare no conflict of interest.

[1]To whom correspondence should be addressed. E-mail: dkennett@uoregon.edu.

*Ages in this paper are expressed in thousands of calendar years before present (ka). Radiocarbon ages will be identified and clearly marked "^{14}C years."

This article contains supporting information online at www.pnas.org/cgi/content/full/0906374106/DCSupplemental.

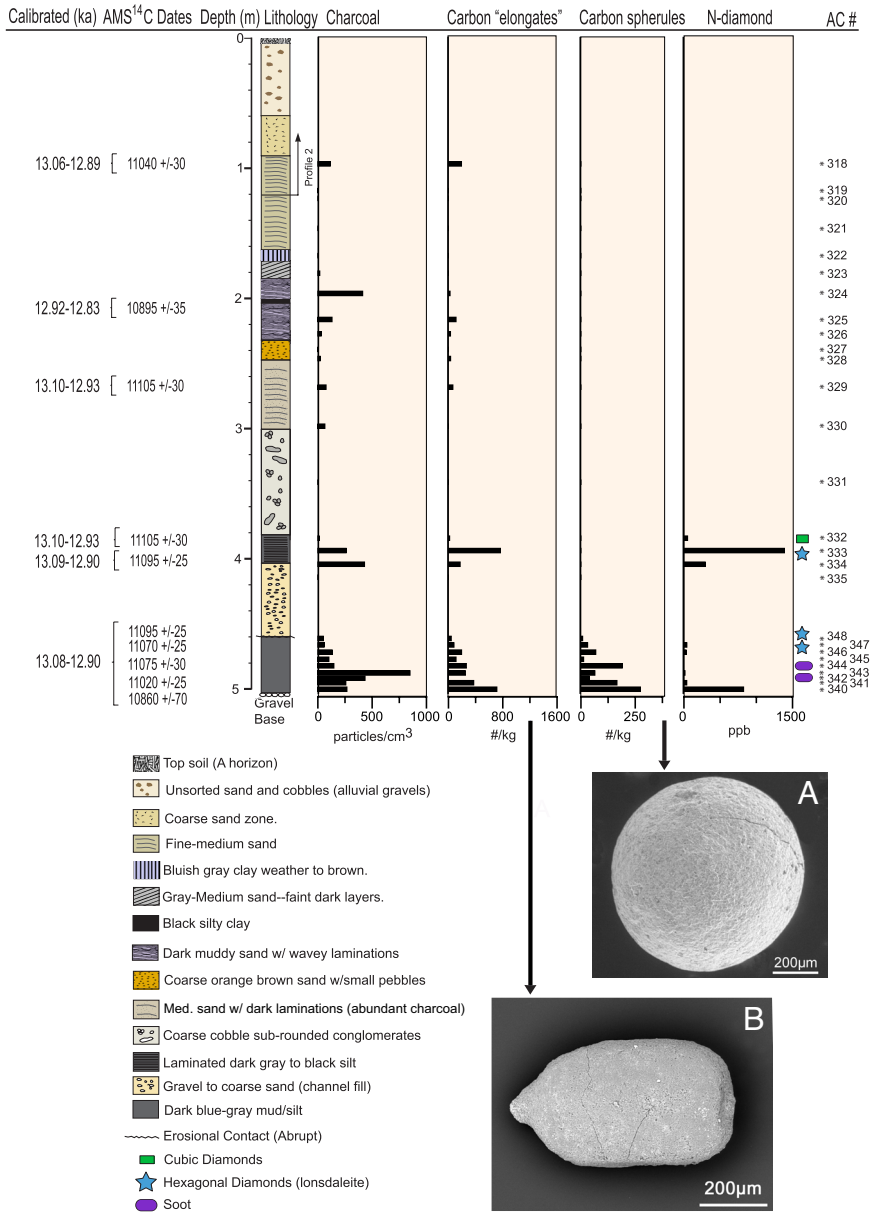

Fig. 1. Stratigraphic section of AC-003 profile (Arlington Canyon, Santa Rosa Island, CA) showing lithology, calibrated and uncalibrated radiocarbon dates, stratigraphic distribution of carbon material (charcoal, elongates, spherules, and soot), and concentrations/locations of 3 different diamond polymorphs (n-diamonds, hexagonal, and cubics). SEM images represent carbon spherules (*A*) and carbon elongates (*B*) from the lower dark sedimentary layers, both of which contain n-diamonds. * designates sediment samples analyzed in this study.

hypothesis. Massive North American animal extinctions could have resulted from the direct effects of these airbursts/impacts (shockwaves, heat, wildfires) and subsequent cascading ecological changes associated with landscape and biotic disruption, interruption of North Atlantic thermohaline circulation, abrupt climate change, and human predation on remnant animal populations. Skepticism about the YDB impact hypothesis has resulted from the absence in the YDB of some widely accepted impact markers that are present in the K/T and other documented impacts (e.g., shocked minerals, breccias, tektites, and a visible impact crater) (15). However, such markers also appear absent from an observed and widely accepted cosmic impact event, the Tunguska airburst over Siberia in 1908 (16).

Results

Here, we present evidence for shock-synthesized hexagonal nanodiamonds (lonsdaleite) in YDB sediments in North America. These diamonds occur at Arlington Canyon on Santa Rosa Island (California), which, at 12.9 ka, was joined with 3 other Northern Channel Islands to form one landmass, Santarosae (Fig. S1*B*) (17). The diamonds occur in a discrete layer that is contemporary with, and similar to, the organic-rich sedimentary layers described by Haynes across North America (see Fig. S1*A*) (5). The best known geological exposure (AC-003) of this dark sedimentary unit is 1.35 km from the modern coastline on the west side of the canyon (Universal Transverse Mercator: 10S 0762524/3764532), where a 44-cm-thick, organic-rich, dark blue-gray, silty mud (black layer) rests directly on a gravel deposit at 5 m (Fig. 1) (18). This layer is capped with a coarse cobble lag deposit (≈60 cm thick) and a second less dark layer of gray to black laminated sandy silt. The rest of the overlying sequence consists of alluvial sands and gravels. Accelerator mass spectrometry (AMS) ^{14}C dates from upper and lower parts of the sequence are statistically similar,

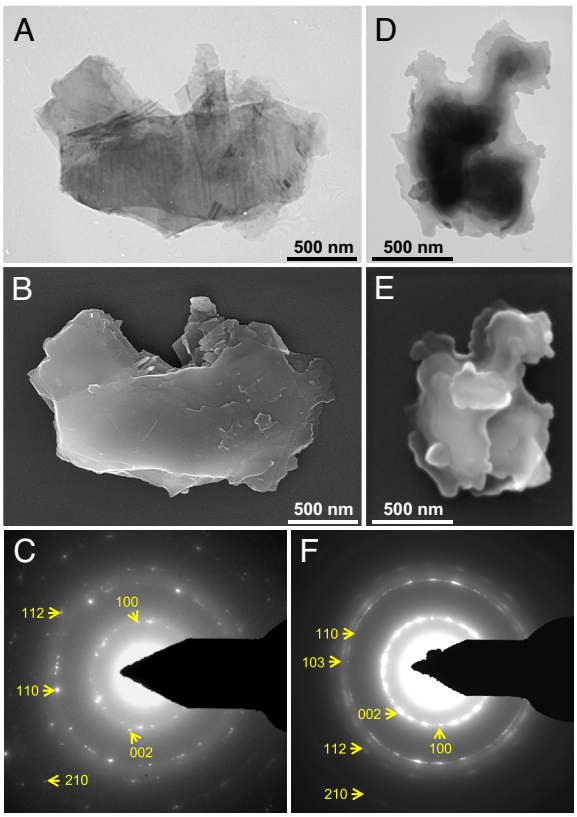

Fig. 2. TEM photomicrographs, SEM images, and diffraction patterns of stacked diamond clusters. TEM photomicrographs (*A* and *D*), SEM images (*B* and *E*), and diffraction patterns (*C* and *F*) of 2 stacked diamond clusters composed primarily of lonsdaleite crystals from the YDB (12.95 ± 0.05 ka) sedimentary layer in Arlington Canyon (AC-003). Both lonsdaleite clusters are from AC-003: 4.59–4.64 m (AC#348). See Fig. 1 for location and Figs. S2–S4 for additional images and information.

suggesting rapid accumulation of fluvial deposits shortly after ~12.95 ± 0.05 ka (18).

Diamonds with hexagonal crystallographic modification were observed only within the lower 2 dark sedimentary layers between 3.92–4.69 m below the modern ground surface. In these stratigraphic units, we discovered both single crystals and clusters of lonsdaleite ranging in size from 20 to 1,800 nm that were either inside or adhered to elongate carbon particles common in these lowest deposits (Fig. 2 and Figs. S2–S6). Transmission electron microscopy (TEM) work demonstrates that these diamonds are mono- and polycrystalline, with some displaying individual lamellae spaced at ≈20–30 nm (Fig. S2). Electron diffraction analyses at multiple locations across these crystals confirm the hexagonal diamond polymorph with reflections corresponding to lattice planar spacings of 2.18, 1.26, 1.09, and 0.826 Å. Tabular (flake-like) morphology and stacking faults in these lonsdaleite crystals are consistent with impact-related shock transformation, in which graphite is the likely parent material (19).

The lonsdaleite in 12.95 ± 0.05 ka sediments at Arlington provides evidence for the presence in the YDB of a shock-synthesized mineral widely considered to be a cosmic impact marker. Controlled experiments indicate that graphite is transformed into a mixture of cubic and hexagonal diamond at ≈15 GPa (2 million psi) at temperatures between 1,000–1,700 °C followed by rapid quenching (19). Lonsdaleite has never been found associated with mantle-derived kimberlitic diamonds (19) and has only been found on Earth inside meteorites (20) and

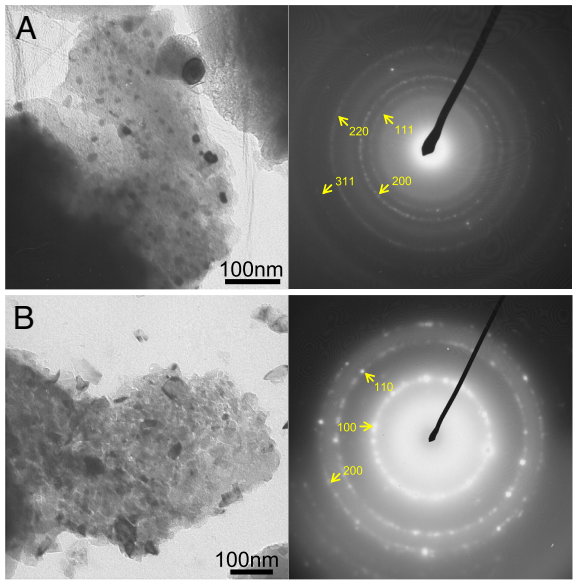

Fig. 3. Paired TEM photomicrographs (*Left*) and diffraction patterns (*Right*) of other diamond polymorphs in the YDB sedimentary layer in Arlington Canyon (AC-003). (*A*) n-diamonds embedded in carbonaceous matrix of a carbon spherule (AC#341); (*B*) a cubic diamond cluster in a carbon elongate (AC # 332). See Fig. 1 for stratigraphic position of samples.

associated with impact craters [e.g., Popigai (21), Reis (22, 23), (Fig. S7)]. These observations make the presence of lonsdaleite an excellent shock indicator (19) and, by extension, a cosmic impact proxy when found in sediments.

The lonsdaleite crystals at Arlington co-occur with carbon spherules and other diamond polymorphs known to be concentrated in 12.9 ± 0.1 ka sediments at multiple locations across North America (13). Carbon spherules (400–1,500 μm) were found in the Arlington sequence only between 4.6–5 m below the ground surface in the lowest dark stratum (black layer) (Fig. 1). Scanning electron microscope (SEM) work shows that the carbon spherules have a characteristic reticulate interior (Fig. S6 *E* and *F*), and a TEM study revealed conspicuous subrounded, spherical, and octahedral crystalline particles (2–300 nm) distributed in their carbonaceous matrices (Fig. 3). Analysis of the particles by electron diffraction shows reflections consistent with cubic diamonds (2.06, 1.26, and 1.07 Å), as well as "forbidden" reflections at 1.78, 1.04, and 0.796 Å, indicative of a metastable "new-diamond" polymorph or n-diamond (24), which has been created in experimental TNT explosions (25), and is known from meteorites (26), but not known to be associated with mantle-derived diamonds. The forbidden reflections are attributed to flaws in the normal cubic diamond lattice (24), perhaps due to rapid quenching consistent with anoxic conditions associated with the shockwave. N-diamonds are abundant in YDB sediments across North America (13), occurring at Arlington in concentrations of ≤1,340 ppb (Fig. 1 and Table S1), equivalent to >1 billion diamonds per cm^3, a concentration comparable to those of cubic diamonds at some K/T boundary localities (3,200 ppb) (27). At Arlington, there is no evidence of upslope diamondiferous sources (e.g., older impact craters) that might have contributed reworked diamonds, and their presence cannot be due to volcanism, because high temperatures (420–570 °C) under oxidizing conditions destroy diamonds (26, 27).

N-diamonds also occur within the matrices of the carbon "elongates" associated with lonsdaleite crystals between 3.92–4.69 m (see Fig. 1). Carbon elongates differ from the carbon spherules in having an irregular array of walls and voids, whereas

carbon spherule interiors display a well-organized honeycomb (reticulated) pattern. Both types are composed entirely of glass-like amorphous carbon indicative of high-temperature formation. The general shape of elongates ranges from angular (hexagonal in cross-section) to subrounded. The elongates were found throughout the sequence, but are concentrated in the lower organic-rich layers below 3.83 m, where they are generally more highly vitrified, hard, and brittle (Fig. S5 and Fig. S6). N-diamonds were found in these elongates only below 3.83 m.

During this TEM survey, clusters of stable cubic diamonds (≈1,000 in total) were found with carbon elongates between 3.83 and 3.86 m. These diamonds appear more angular than the associated n-diamonds and have diffraction patterns typical of cubic diamonds (2.06, 1.26, 1.08 Å; Fig. 3*B*). Similar cubic diamonds have been identified in YDB sediments at Bull Creek in northwest Oklahoma and Murray Springs, Arizona (13). This diamond polymorph is also found in the ejecta layer of the K/T boundary impact (27, 28) and forms at higher temperatures and pressures than n-diamond, but the conditions of formation for all 3 polymorphs fall outside the range of Earth's known surficial processes. The co-occurrence of lonsdaleite and cubic diamonds with n-diamond at Arlington bolsters the interpretation that the n-diamond polymorph, common in YDB sediments elsewhere in North America (13), is impact-related. However, investigations are needed to determine if the lonsdaleite formed in the high pressure-temperature environment of a surface impact or were transported inside the impactor. Hexagonal diamonds are known to occur in meteorites (e.g., ref. 29; see also Fig. S7), but may not occur in sufficient abundance to account for their presence in the YDB layer. Also, because up to ≈90% of an impactor's mass may be vaporized upon impact, it seems less likely that the abundant hexagonal diamonds at Arlington arrived with the impactor and more likely that they formed upon impact. Due to their plate-like morphology, the hexagonal diamonds most likely formed via shock transformation of graphite, which does not appear to occur locally where they were discovered. However, because nanometer-sized diamonds were distributed widely through the atmosphere during the K/T impact event, it is plausible that the hexagonal diamonds arrived at Arlington after forming in a distant impact into carbon-rich target rocks. Because cosmic isotopic ratios of carbon ($\delta^{13}C$) and nitrogen ($\delta^{15}N$) often have very different values from terrestrial ratios (30), we plan to measure $\delta^{13}C$ and $\delta^{15}N$ content of these hexagonal diamonds to help determine their origin.

Discussion

Shock-synthesized hexagonal diamonds and other nanometer-sized diamond polymorphs also co-occur with high concentrations of charcoal and other forms of particulate carbon (carbon spherules and elongates) that are indicative of major biomass burning at ≈12.95 ± 0.05 ka. In addition, grape-clustered microscopic soot was found (sample AC343, 2,500 ± 250 ppm; Fig. S8 and see Fig. 1 for location) in the lowest deposits at Arlington. Soot is rare in the geological record, but is well-documented in the K/T boundary layer (65 Ma) and other cosmic impact-related deposits (31, 32). Soot is produced in flaming combustion at high temperatures consistent with intense wildfires and the reduction of conifer forests common on these islands at 12.95 ± 0.05 ka (18). The near consistency of AMS ^{14}C ages (at 12.95 ± 0.05 ka) throughout the lower 4 m of the sequence suggests that these intense fires denuded the landscape and promoted sediment mass wasting (18) that rapidly buried the diamonds and soot. The close association of shock-synthesized diamonds with a wide-range of wildfire proxies is consistent with the hypothesis that they were ignited by an intense radiation flux associated with a cosmic impact. The presence of millions of diamonds embedded inside carbon spherules and the rapid burial of these deposits is inconsistent with the alternative hypothesis that micrometeoritic materials accumulated on a stable surface over an extended interval (33).

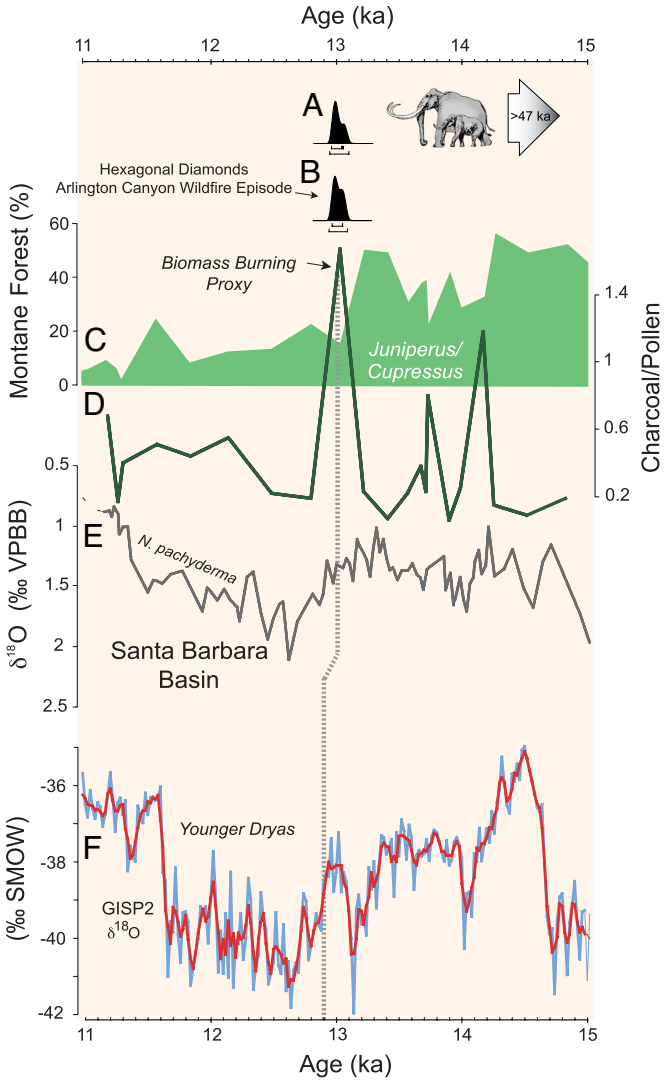

Fig. 4. Summary of climate change, vegetational shifts, and *Mammuthus exilis* (Pygmy Mammoth) extinction at the YDB shown relative to the age of hexagonal diamonds in Arlington Canyon and regional biomass burning proxies. Comparison of the known terminal age of *M. exilis* (*A*) and age of Arlington Canyon hexagonal diamonds and major YDB wildfire episode (*B*) with other proxies in Santa Barbara Basin between 15 and 11 ka; (*C*) percent abundance of montane forest types (*Juniperus-Cupressus*) (29); (*D*) ratio of pollen to charcoal concentration in Santa Barbara Basin (34); (*E*) $\delta^{18}O$ record of *Neogloboquadrina pachyderma* (35); (*F*) Comparative Greenland Ice Sheet (GISP2) $\delta^{18}O$ record (36) with heavy gauge lines representing splines of raw data. Santa Barbara Basin chronology is from ref. 35. Gray dashed line marks the initiation of the Younger Dryas cooling event in Greenland and Santa Barbara Basin, an event considered synchronous between these records. Drawing shows the size of *M. exilis* compared with *M. columbi* of the North American continent (illustration by Rusty Van Rossman).

Biomass burning in Arlington Canyon is synchronous with wildfires elsewhere on the Channel Islands at ≈12.95 ± 0.05 ka (18) and contemporary with the largest of several peak burning events in the last 25,000 years recorded in nearby Santa Barbara Basin Ocean Drilling Program [Site 893 (34); Fig. 4 and see Fig. S1 for core location]. Increase in ballast minerals and higher sedimentation rates in the Santa Barbara Basin at 12.95 ± 0.05

ka (35) are also consistent with sediment mass wasting of a denuded landscape in the wake of extensive biomass burning on the adjacent islands and mainland (18). This well-dated marine sequence also records a shift to Younger Dryas (YD) cooling (36, 37) and relatively abrupt vegetational change from closed montane forest to more open habitats dominated by grasslands, chaparral, and dispersed oak stands, the dominant regional vegetation throughout the YD and Holocene (34, 38).

The unique combination of high-resolution terrestrial and marine sedimentary records from the Northern Channel Islands and adjacent Santa Barbara Basin indicate regional wildfire and abrupt ecological disruption. This disruption coincides with the last known occurrence of pygmy mammoths on Santarosae (*Mammuthus exilis*, ≈12.95 ± 0.05 ka, Fig. 4*A*) (39) and the beginning of a gap of 600–800 years in the archaeological record (18, 40). The distinctive dark layer in Arlington Canyon correlates in time with the base of other dark sedimentary layers distributed across North America that contain nanometer-sized diamonds and evidence for biomass burning (12, 13). This biomass burning appears coeval with evidence from the Greenland ice sheet for an abrupt increase in hemispheric wildfires at the beginning of the YD (41, 42, contra 43). The base of the black layer (YDB) in North America marks a major biostratigraphic change; the remains of extinct megafaunal taxa occur directly below and never above this readily discernable layer (5). This observation is consistent with radiocarbon evidence indicating abrupt extinction of mammoths and 15 other North American animal genera (5, 6). The vast majority of the North American megafaunal taxa abruptly vanished from the North American continent at the onset of the YD at 12.9 ± 0.1 ka, as marked by a major stratigraphic boundary layer that is rich in nanodiamonds (13). The uniqueness of this megafaunal extinction is highlighted by the evolutionary history of the horse, which had lineages continuously present in North America since their appearance in the early Cenozoic at about 55 Ma (44) except after 12.9 ± 0.1 ka when *Equus* suddenly disappeared from the continent (5). Before the YDB, the last known major comprehensive and abrupt megafaunal extinction recorded in North America occurred at the K/T boundary (65 Ma). Both the K/T and YDB events are uniquely similar through their association of megafaunal extinction with a distinct layer that is rich in nanodiamonds and soot. The presence of shock-synthesized hexagonal and other nanometer-sized diamonds in YDB sediments in association with soot and other wildfire indicators is consistent with a cosmic impact event at 12.9 ± 0.1 ka, and the hypothesis that the Earth crossed paths with a swarm of comets or carbonaceous chondrites producing airshocks and/or surface impacts that contributed to abrupt ecosystem disruption and megafaunal extinctions in North America.

Methods

The carbon particles (spherules, elongates, and charcoal) were separated by flotation and hand-picking. For analysis, standard techniques were used for TEM and SEM imaging, including energy dispersive x-ray spectroscopy (EDS) and electron energy loss spectroscopy (EELS). Selected particles (10–15) were collectively crushed and dispersed on a TEM grid for diamond analytical work (see *SI Methods*), and the allotropes were identified by using standard crystallographic diffraction patterns. Soot was separated and identified by using standard techniques (31).

ACKNOWLEDGMENTS. We appreciate the comments of 2 anonymous reviewers, resulting in valuable improvements to the manuscript. Early support from the Office of Research at the University of California, Santa Barbara and the University of Oregon is greatly appreciated. We thank Channel Islands National Park for logistical support; Don Morris for assistance in the field; John and Jennifer Donovan and other staff at the Lorry I. Lokey Nanotechnology Laboratories at University of Oregon, and the FEI Company for their generous support and technical assistance. This work also made use of Materials Research Laboratory Central Facilities supported by the Materials Research Science and Engineering Centers Program of the National Science Foundation under Award DMR05 and the Scanning Electron Microscope facilities of D. Morse at University of California, Santa Barbara. This research was funded by the National Science Foundation (ATM-0713769; also GRFP-2006022778 to B.J.C.) and Bray (D.J.K.) and Knight (J.M.E.) fellowships at the University of Oregon.

1. Grayson DK (2007) Deciphering North American Pleistocene extinctions. *J Anthropol Res* 63:185–213.
2. Martin PS (2005) *Twilight of the Mammoths: Ice Age Extinctions and the Rewilding of America* (University of California Press, Berkeley, CA).
3. Drummond AJ, Rambaut A, Shapiro B, Pybus OG (2005) Bayesian coalescent inference of past population dynamics from molecular sequences. *Mol Biol Evol* 22:1185–1192.
4. Grayson DK (1987) The biogeographic history of small mammals in the Great Basin: Observations on the last 20,000 years. *J Mammal* 68:359–375.
5. Haynes CV, Jr (2008) Younger Dryas "black mats" and the Rancholabrean termination in North America. *Proc Natl Acad Sci USA* 105:6520–6525.
6. Fiedel S (2008) in *American Megafaunal Extinctions at the End of the Pleistocene*, ed Haynes G (Springer, The Netherlands), pp 21–37.
7. Grayson DK, Meltzer DJ (2003) A requiem for North American overkill. *J Archaeol Sci* 30:585–593.
8. Yule JV, Jensen CXJ, Joseph A, Goode J (2009) The puzzle of North America's Late Pleistocene megafaunal extinction patterns: Test of new explanation yields unexpected results. *Ecol Mod* 220:533–544.
9. Anderson A (1989) Mechanics of overkill in the extinction of New Zealand moas. *J Archaeol Res* 16:137–151.
10. Steadman DW (1995) Prehistoric extinctions of Pacific island birds: Biodiversity meets zooarchaeology. *Science* 267:1123–1130.
11. Barnosky AD, Koch PL, Feranec RS, Wing SL, Shabel AB (2004) Assessing the causes of Late Pleistocene extinctions on the continents. *Science* 306:70–75.
12. Firestone RB, et al. (2007) Evidence for an extraterrestrial impact 12,900 years ago that contributed to the megafaunal extinctions and Younger Dryas cooling. *Proc Natl Acad Sci USA* 104:16016–16021.
13. Kennett DJ, et al. (2009) Nanodiamonds in Younger Dryas boundary sediment layer. *Science* 323:94.
14. Alvarez LW, Alvarez W, Asaro F, Michel HV (1980) Extraterrestrial cause for the Cretaceous-Tertiary extinction. *Science* 208:1095–1108.
15. Köeberl C (2007) The geochemistry and cosmochemistry of impacts. *Treatise on Geochemistry*, ed Davis A (Elsevier, Amsterdam, The Netherlands), Vol 1, pp 1–52.
16. Longo G, Serra R, Cecchina S, Galli M (1994) Search for microremnants of the Tunguska cosmic body. *Planet Space Sci* 42:163–177.
17. Orr PC (1968) *Prehistory of Santa Rosa Island* (Santa Barbara Museum of Natural History, Santa Barbara, CA).
18. Kennett DJ, et al. (2008) Wildfire and abrupt ecosystem disruption on California's Northern Channel Islands at the Ållerød-Younger Dryas boundary (13.0–12.9 ka). *Quaternary Sci Rev* 27:2528–2543.
19. DeCarli PS, Bowden E, Jones AP, Price GD (2002) in *Catastrophic Events and Mass Extinctions: Impacts and Beyond*, eds Koeberl C, MacLeod K (Geological Society of America Special Paper 356, Boulder, CO), pp 595–605.
20. Hanneman RE, Strong HM, Bundy FP (1967) Hexagonal diamonds in meteorites: Implications. *Science* 155:995–997.
21. Köeberl C, et al. (1997) Diamonds from the Popigai impact structure, Russia. *Geology* 25:967–970.
22. Oleinik GS, Valter AA, Erjomenko GK (2003) The structure of high pressure lonsdaleite diamond grains from the impactites of the Belilovka (Zapadnaja) astrobleme (Ukraine). *34th Annual Lunar and Planetary Science Conference, March 17–21, 2003* (League City, Texas), 1561 (abstr).
23. Langenhorst F, Shafranovsky G, Masaitis VL (1998) A comparative study of impact diamonds from the Popigai, Ries, Sudbury, and Lappajärvi craters. *Meteorit Planet Sci* 33:A90 (abstract 5083).
24. Wen B, et al. (2007) Synthesis and crystal structure of n-diamond. *Int Mater Rev* 52:131–151.
25. Yamada K, Sawaoka AB (1994) Very small spherical crystals of distorted diamond found in a detonation product of explosive/graphite mixtures and their formation mechanism. *Carbon* 324:665–673.
26. Grady MM, Lee MR, Arden JW, Pillinger CT (1995) Multiple diamond components in Acfer 182. *Earth Planet Sc Lett* 136:677–692.
27. Hough RM, et al. (1995). Diamonds from the iridium-rich K-T boundary layer at Arroyo el Mimbral, Tamaulipas, Mexico. *Geology* 25:1019–1022.
28. Carlisle BC, Braman RB (1991) Nanometre-size diamonds in the Cretaceous/Tertiary boundary clay of Alberta. *Nature* 352:708–709.
29. Jenniskens P, et al. (2008) The impact and recovery of asteroid 2008 TC3. *Nature* 458:485–488.
30. Gilmour I, et al. (1992) Terrestrial carbon and nitrogen isotopic ratios from Cretaceous-Tertiary boundary nanodiamonds. *Science* 258:1624–1626.
31. Wolbach WS, Lewis RS, Anders E (1985) Cretaceous extinctions: Evidence for wildfires and search for meteoritic impact. *Science* 230:167–170.
32. Wolbach WS (1990) Carbon across the Cretaceous-Tertiary boundary. PhD thesis, (Univ of Chicago, Chicago).

33. Pinter N, Ishman SE (2008) Impacts, mega-tsunami, and other extraordinary claims. *GSA Today* 18:37–38.
34. Heusser LE, Sirocko F (1997) Millennial pulsing of environmental change in southern California from the past 24 k.y.: A record of Indo-Pacific ENSO events? *Geology* 25:243–246.
35. Nederbragt AJ, Thurow JW, Bown PR (2008) Paleoproductivity, ventilation, and organic carbon burial in the Santa Barbara Basin (ODP site 893, off California) since the last glacial. *Paleoceanography* 23:1–15.
36. Hendy IL, Kennett JP, Roark EB, Ingram BL (2002) Apparent synchroneity of submillennial scale climate events between Greenland and Santa Barbara Basin, California from 30–10 ka. *Quaternary Sci Rev* 21:1167–1184.
37. Stuiver M, Grootes PM (2000) GISP2 oxygen isotope ratios. *Quaternary Res* 53:277–283.
38. Heusser L (1998) Direct correlation of millennial-scale changes in western North America vegetation and climate with changes in the California current system over the past ~60 kyr. *Paleoceanography* 19:1–15.
39. Agenbroad LD, Johnson JR, Morris D, Stafford TW, Jr (2005) in *Proceedings of the Sixth California Islands Symposium*, eds Garcelon DK, Schwemm CA (Institute for Wildlife Studies, Arcata, CA), pp 3–7.
40. Johnson JR, Stafford TW Jr, Ajie HO, Morris DP (2002) in *Proceedings of the Fifth California Islands Symposium*, eds Browne DR, Mitchell KL, Chaney HW (Santa Barbara Museum of Natural History, Santa Barbara, CA), pp 541–545.
41. Mayewski PA, et al. (1993) The atmosphere during the Younger Dryas. *Science* 261:195–197.
42. Mayewski PA, et al. (1997) Major features and forcing of high-latitude northern hemisphere atmospheric circulation using a 110,000-year-long glaciochemical series. *J Geophys Res* 102:26345–26366.
43. Marlon JR, et al. (2009) Wildfire responses to abrupt climate change in North America. *Proc Natl Acad Sci USA* 106:2519–2524.
44. MacFadden BJ (2008) *Fossil Horses: Systematics, Paleobiology, and Evolution of the Family Equidae* (Cambridge Univ Press, New York).

Supporting Information

Kennett et al. 10.1073/pnas.0906374106

SI Methods

Incremental sediment samples from the Arlington Canyon geological section (AC-003) were dried and weighed. Sediments were then disaggregated, and "elongate" and spherical carbon particles were extracted via flotation and hand picked using a light microscope. Carbon elongates (≈10–15) and spherules from each stratum were grouped and crushed to a powder in 3.7-mL glass vials and mixed with 4–5 drops of 100% alcohol (ETOH) to suspend the carbonaceous powder. This admixture was pipeted to a 200-mesh copper TEM grid and dried. A representative random sample of grid cells (≈5%) was scanned for diamonds with JEOL 1200EX II, JEOL 1210, or FEI Titan transmission electron microscopes. A TEM was used to identify and image single and clustered crystals, and the diamond polymorphs were identified via selected area electron diffraction. Diamonds ranged in size between 2–1,500 nm, and crystallographic work was restricted to clusters of small crystals or larger single crystals capable of producing diffraction patterns. Multiple measurements were taken across large diamonds to determine purity. Low electron beam voltages (60–80 kV) were used because n-diamonds and lonsdaleite are metastable and vaporize at high temperatures. N-diamond concentrations inside carbon spherules were calculated using the volume of bulk sediment, the average diameter of the carbon spheres in each level, the percentage containing n-diamonds, the percentage by volume of n-diamonds in carbon spherules, and the average size of n-diamonds. Standard techniques were used for scanning electron microscope imaging. EDS and EELS analysis demonstrated that the nanoparticles identified as diamonds via selected area diffraction contain only carbon.

Soot samples were extracted and analyzed using standard procedures described by Wolbach (1, 2). Sediment samples were dried, weighed, and then demineralized using alternating 9 M HCl and 10 M HF/1 M HCl treatments to dissolve carbonates and silicates. The resultant carbonaceous residue was oxidized for 600 h with 0.2 M $Na_2Cr_2O_7$/2.0 M H_2SO_4 to selectively destroy organic carbon. The elemental carbon residue was dried, weighed, and examined on the SEM, where any soot particles present were identified by their characteristic aciniform ("bunch of grapes") morphology and quantified using image particle size analysis.

1. Wolbach WS, Lewis RS, Anders E (1985) Cretaceous extinctions: Evidence for wildfires and search for meteoritic impact. *Science* 230:167–170.
2. Wolbach WS (1990) Carbon across the Cretaceous-Tertiary boundary. PhD thesis, (Univ of Chicago, Chicago).
3. Haynes CV, Jr (2008) Younger Dryas "black mats" and the Rancholabrean termination in North America. *Proc Natl Acad Sci USA* 105:6520–6525..
4. Kennett DJ, et al. (2008) Wildfire and abrupt ecosystem disruption on California's Northern Channel Islands at the Ållerød-Younger Dryas boundary (13.0–12.9 ka). *Quaternary Sci Rev* 27:2528–2543.
5. Oleinik GS, Valter AA, Erjomenko GK (2003) The structure of high pressure lonsdaleite diamond grains from the impactites of the Belilovka (Zapadnaja) astrobleme (Ukraine). *34th Annual Lunar and Planetary Science Conference, March 17-21, 2003* (League City, Texas), 1561 (abstr).

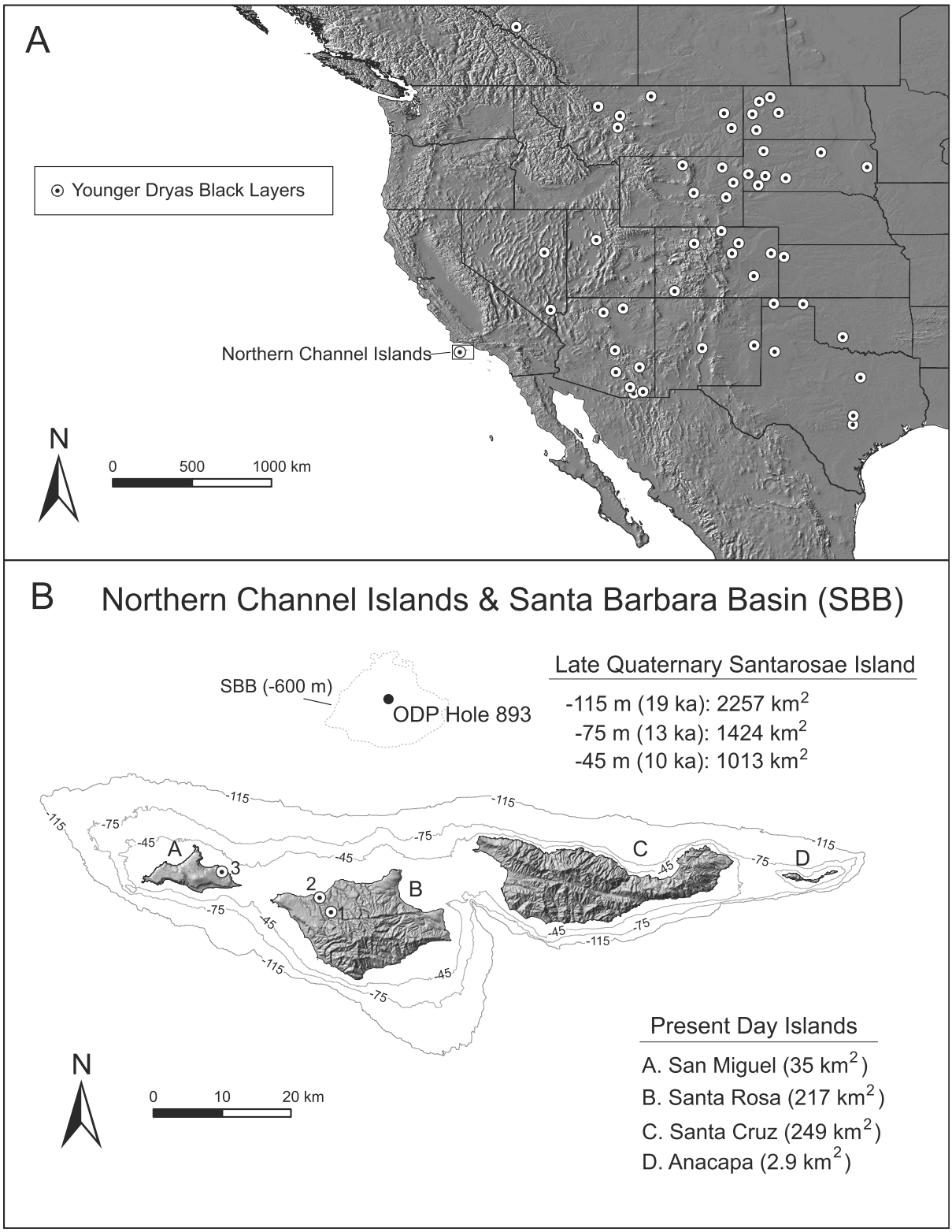

Fig. S1. Maps of western North America and Northern Channel Islands showing localities discussed in the text. (*A*) The distribution of black sedimentary layers in western North America is based on Haynes (3). (*B*) See Kennett et al. (4) for details about the bathymetry surrounding the Northern Channel Islands. Localities identified on the Northern Channel Islands are indicated by numbers: 1, Arlington Canyon (AC-003); 2, Arlington Springs Human locality (CA-SRI-173); 3, Daisy Cave. (Figure layout by Jacob Bartruff.)

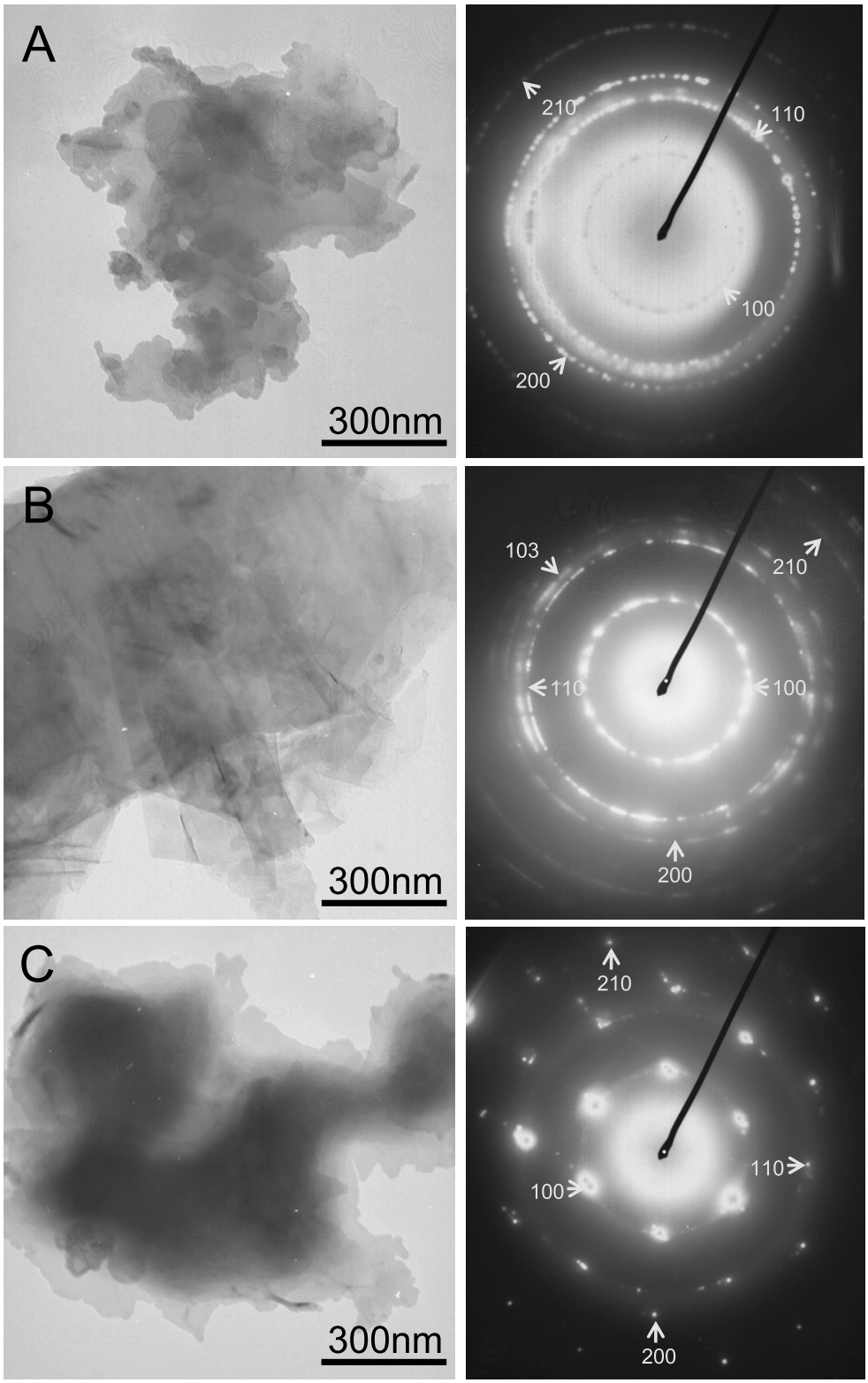

Fig. S2. Additional TEM photomicrographs (*Left*) and diffraction patterns (*Right*) of hexagonal diamond polymorphs in the YDB (12.95 ± 0.05 ka) sedimentary layer in Arlington Canyon (AC-003). (*A*) Cluster of lonsdaleite crystals and associated diffraction pattern from 4.64 and 4.69 m (AC#347); (*B*) cluster of lonsdaleite crystals and associated diffraction pattern from 4.59–4.64 m (AC#348); (*C*) close-up of single lonsdaleite crystal and associated diffraction pattern from 4.59–4.64 m (AC#348)—note lamellae. See Fig. 1 for stratigraphic position of samples.

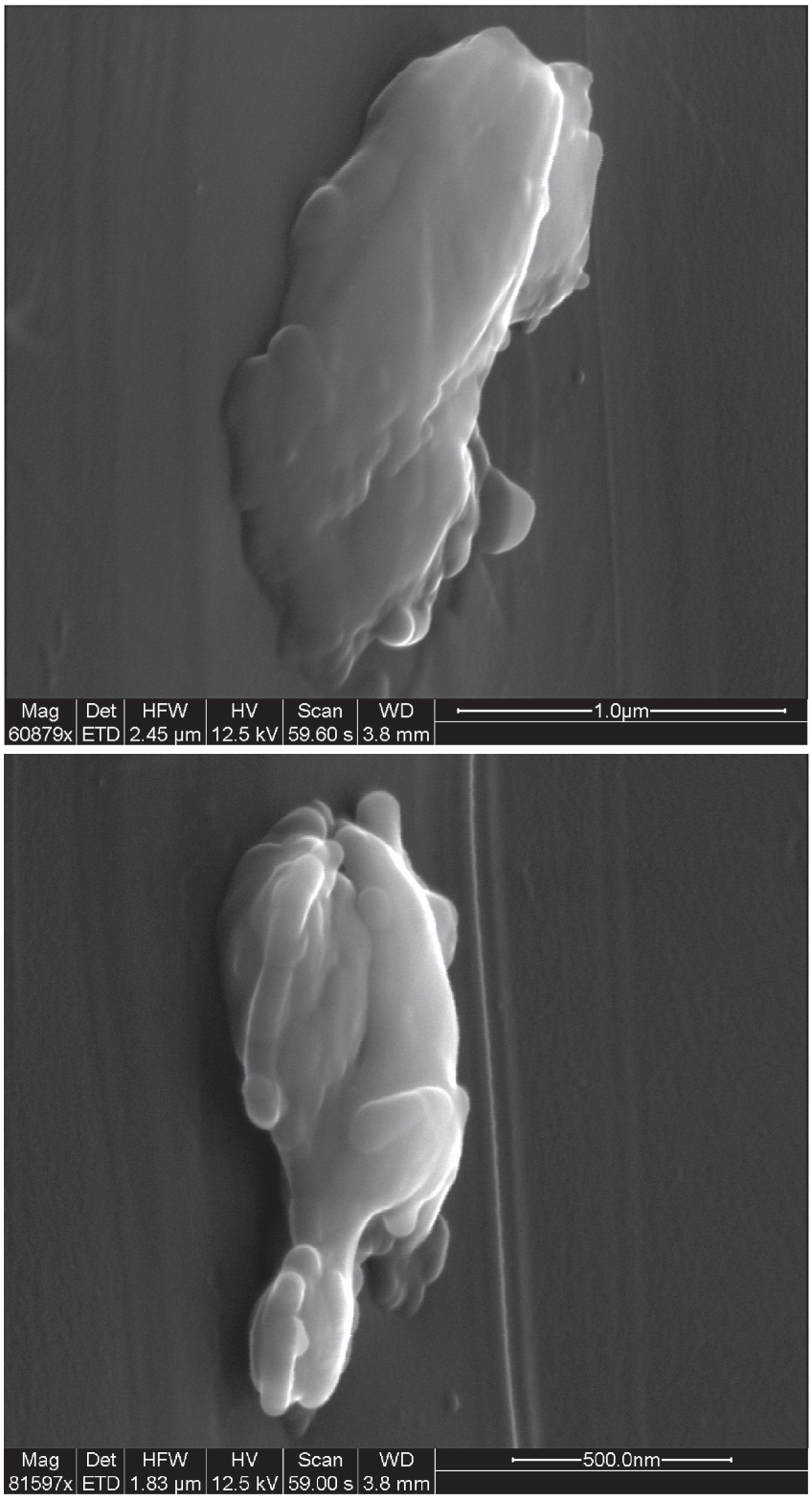

Fig. S3. Oblique SEM images of lonsdaleite crystal clusters shown in Fig. 2.

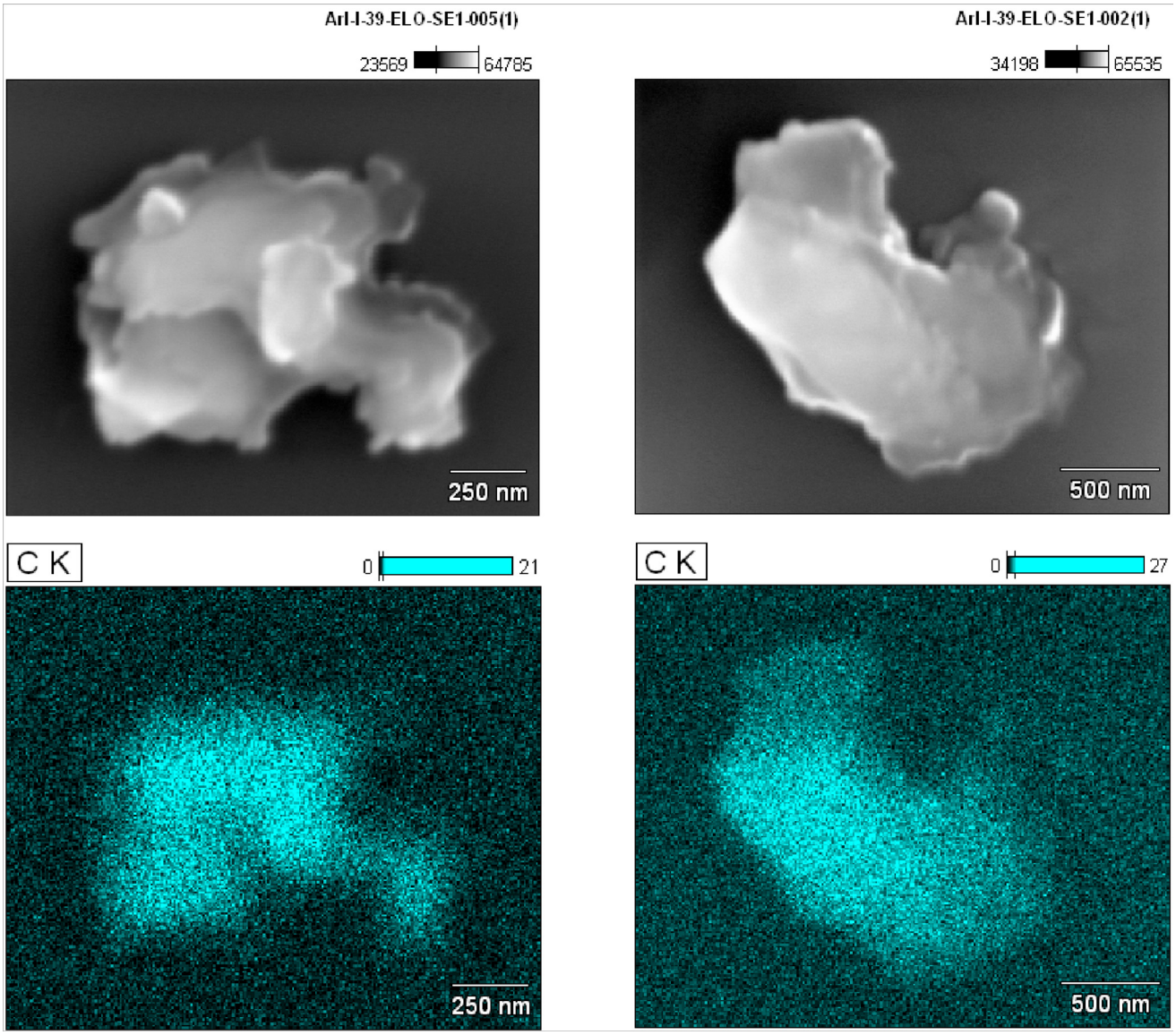

Fig. S4. Image map of EDS spectra of lonsdaleite crystal clusters shown in Fig. 2 that demonstrates dominant carbon composition.

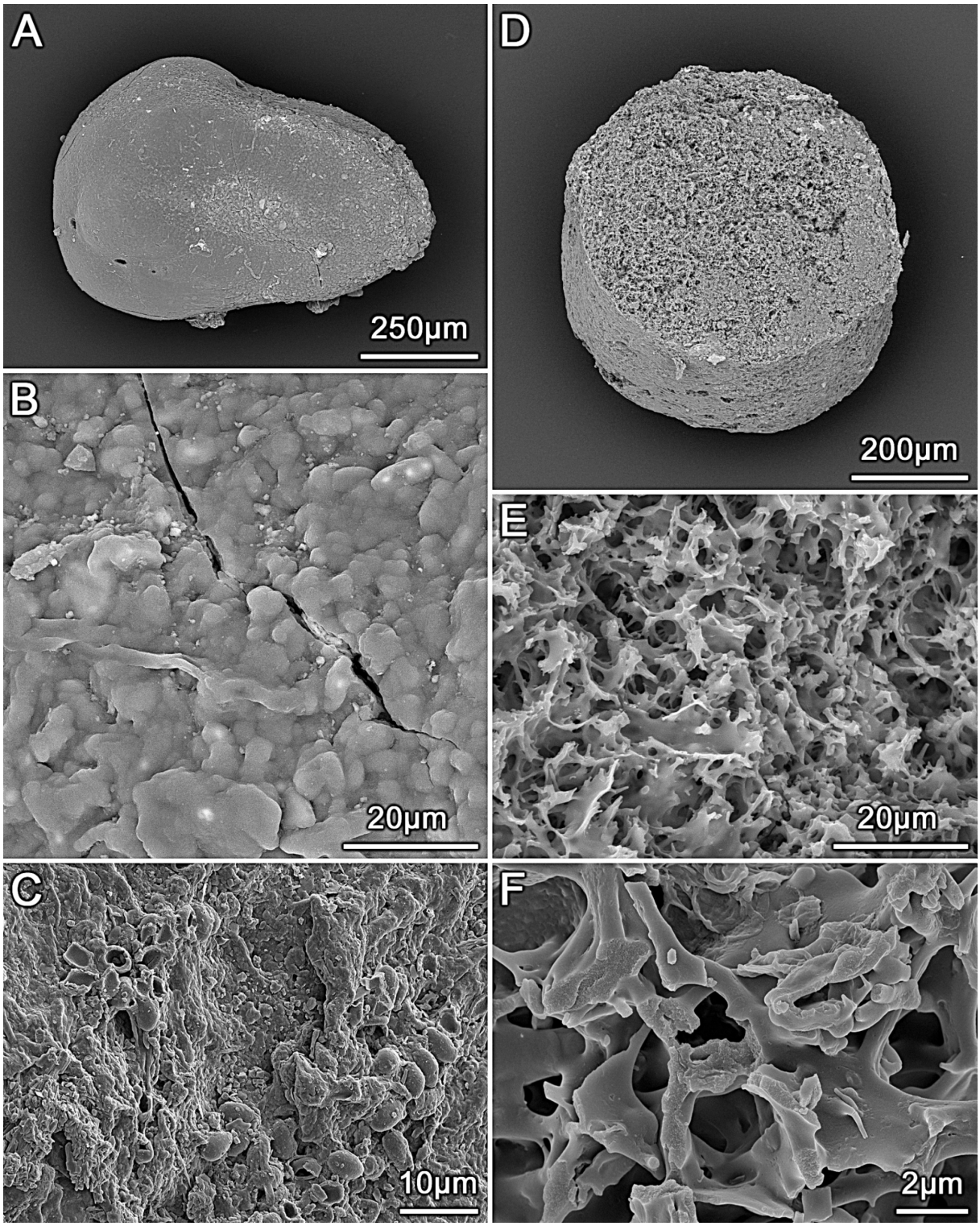

Fig. S5. SEM images of carbon elongates from YDB layer in Arlington Canyon Section, Santa Rosa Island, California (basal black layer). (*A*) Large, subangular carbon elongate showing smooth and glassy surface. (*B*) Surface microstructure at about midpoint (to the left) of elongate in *A* showing relatively smooth relief (botryoidal texture) due to melting. (*C*) Surface microstructure of edge (to the right) of carbon elongate shown in *A* showing roughness (with hollow bean-like structures of unknown origin). (*D*) Bisected, carbon elongate with relatively rounded exterior showing interior structure of complex, nonreticulate walls and voids. (*E*) Irregular, complex, nonreticulate interior of carbon elongate shown in *D* that illustrates well-vitrified and brittle thin walls of amorphous carbon separating voids. (*F*) Higher magnification image of complex, irregular interior of same elongate as in *D* and *E*. Walls are made of massive, highly vitreous, amorphous carbon.

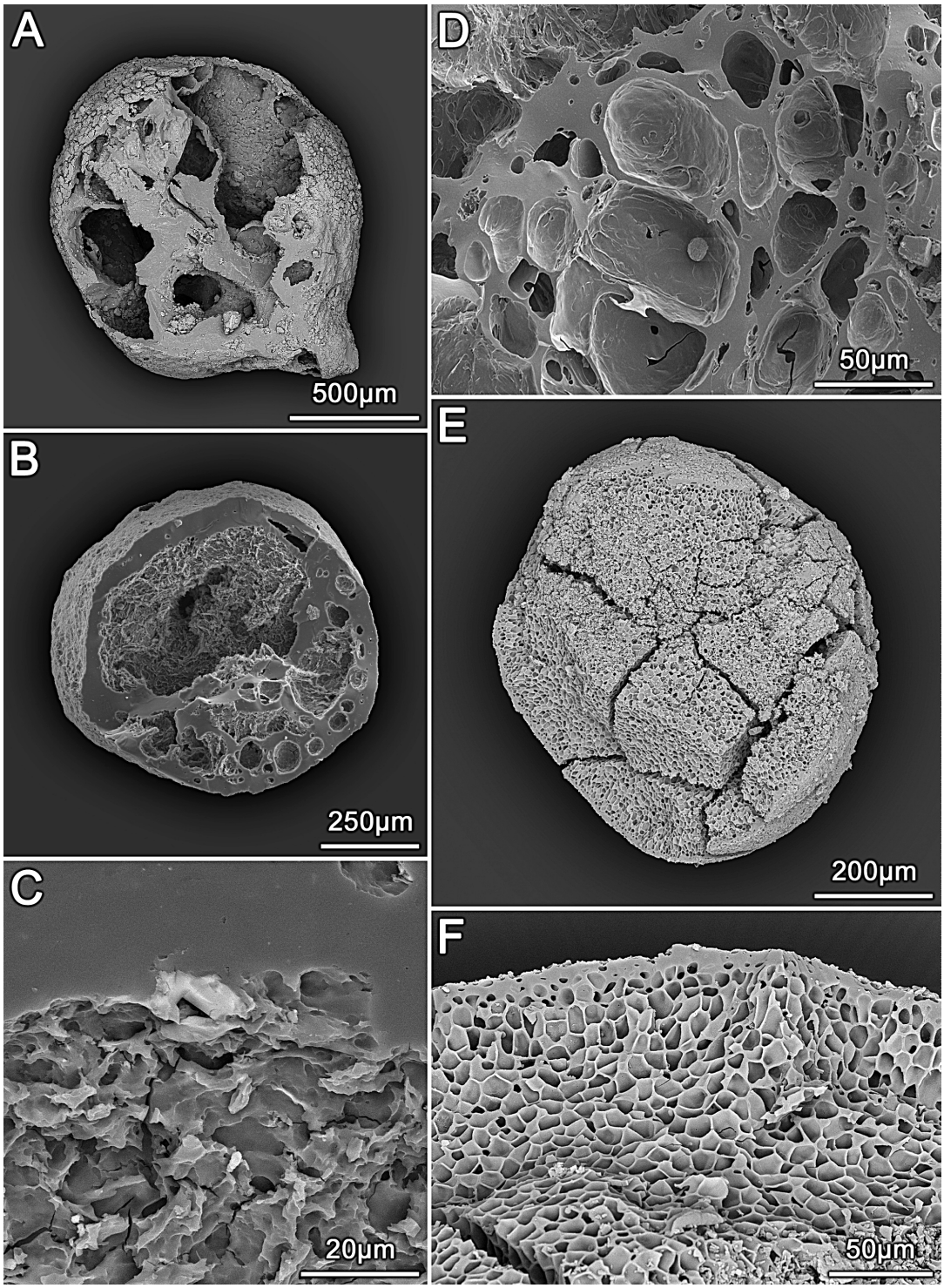

Fig. S6. SEM images of carbon elongates and carbon spherules from YDB layer (basal black layer), Arlington Canyon section, Santa Rosa Island, California. (*A*) Carbon elongate, strongly vitrified walls throughout (surface and interior) containing large voids. (*B*) Bisected carbon elongate, strongly vitrified structure throughout, with thick, massive rind containing voids and hollow center with complex, irregular structure. (*C*) More magnified image of carbon elongate shown in *B* illustrating massive, complex outer crust and irregular, complex interior walls and voids. (*D*) Interior vesicles of strongly vitrified carbon elongate. (*E*) Bisected carbon spherule showing typical internal reticulate (honeycomb) structure and thin, nonreticulate crust. (*F*) Close-up of carbon spherule interior shown in *E* with well-organized reticulate (honeycomb) structure and thin, nonreticulate crust. Carbon spherules differ from carbon elongates by having well-organized, reticulate, rather than irregular, complex interiors.

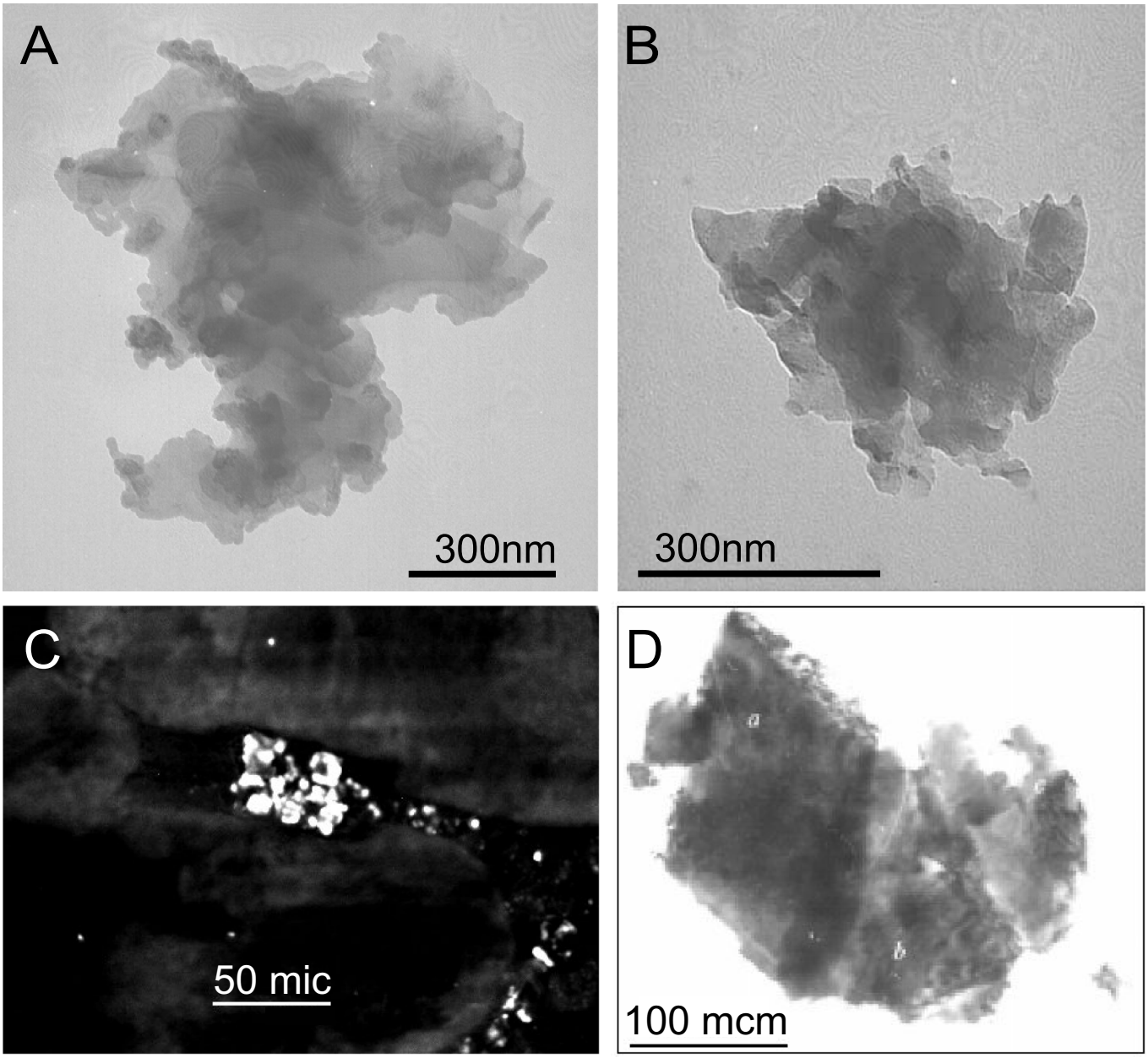

Fig. S7. Images of hexagonal diamond clusters. Diamond clusters were obtained from: (*A*) ≈12.95 ± 0.05 ka deposits in Arlington Canyon (TEM); (*B*) African Ureilite NWA 2971 (TEM); (*C*) African Ureilite NWA 2971 (cathodoluminescence, SEM); (*D*) Belilovka impact crater (5). The SEM image (*C*) shows in situ hexagonal diamonds set in thermally decomposed graphite (dark).

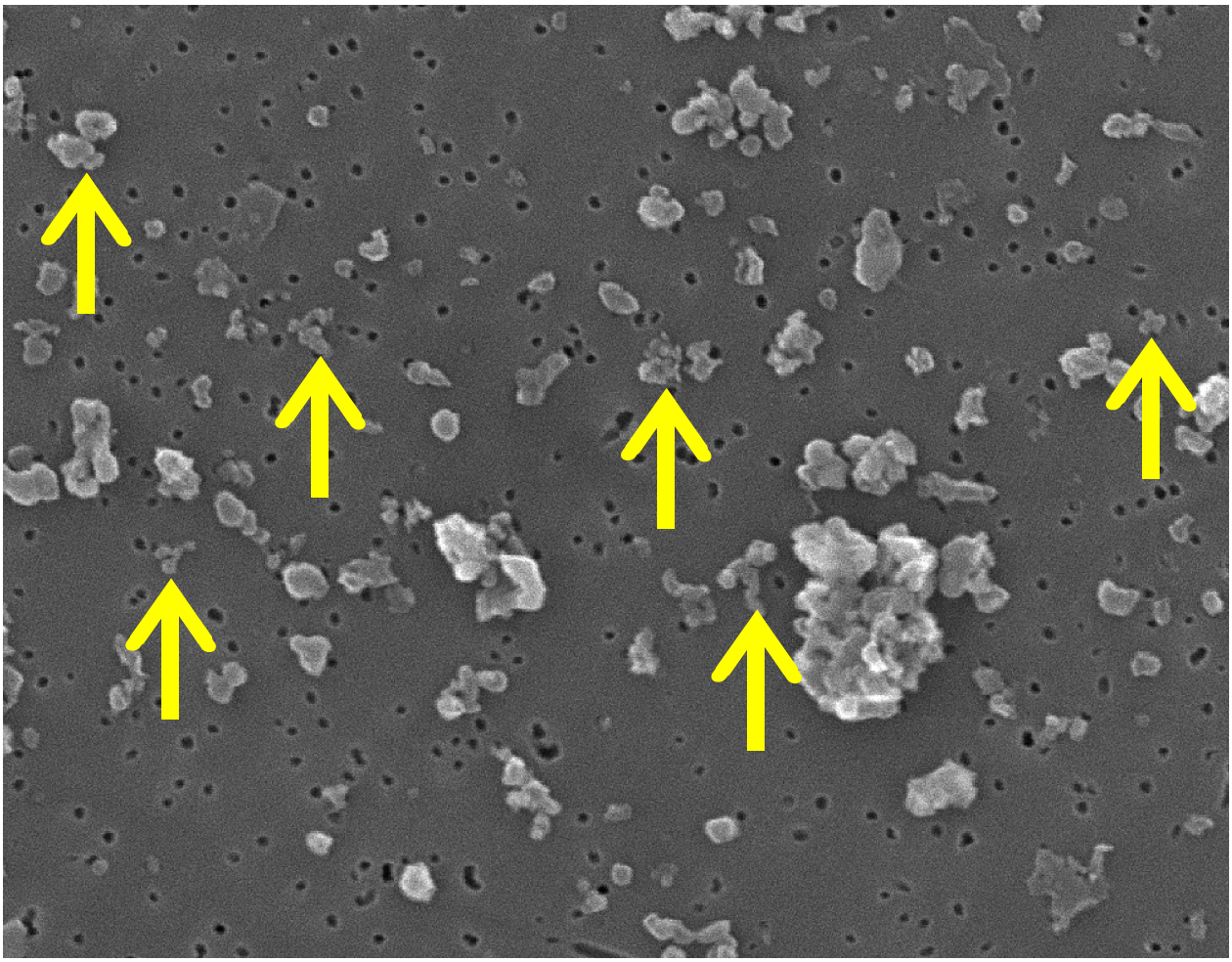

Fig. S8. SEM micrograph of grape-clustered soot (examples marked by yellow arrows) from Arlington Canyon. Highest concentrations were identified in level AC 343 (2,500 ± 250 ppm), with trace amounts found in AC344 (13 ± 1 ppm). High abundances of soot are consistent with impact-triggered fires and sudden burial favoring preservation.

Table S1. Quantitative distribution of organic carbon, other carbon forms (e.g., wood and herbaceous charcoal, various carbon particles, soot), and diamonds in sediment samples from Arlington Canyon (AC-003)

								Diamonds						
			Charcoal		Carbon			N-Diamonds			Cubic	Hexagonal	Soot	
Sample no.	cmbs	% Organic C	Wood no./cm^3	Herbaceous, %	Spherules, no./kg	Elongate, no./kg	Glasslike, g/kg	In CS, ppb*	In Elongate, ppb*	Total, ppb	No. detected	No. detected	ppm	±
AC318	95–99†	1.870	115	7.83	0	192	0.000	0	0	0				
AC319	115–120†	2.080	2	0.00	0	0	0.000	0	0	0				
AC320	122–125	2.044	0	0.00	0	0	0.000	0	0	0				
AC321	145–148	2.601	0	0.00	0	0	0.000	0	0	0				
AC322	166–169	3.870	0	0.00	0	0	0.000	0	0	0				
AC323	179–183	2.175	18	0.00	0	0	0.000	0	0	0				
AC324	195–198	1.991	413	8.72	0	23	0.001	0	0	0				
AC325	215–217	3.459	131	0.00	0	112	0.001	0	0	0				
AC326	226–229	1.920	31	0.00	0	30	0.001	0	0	0				
AC327	238–241	2.437	2	0.00	0	0	0.000	0	0	0				
AC328	245–248	1.416	22	0.00	0	31	0.001	0	0	0				
AC329	267–270	1.688	76	1.32	0	66	0.000	0	0	0				
AC330	297–300	2.838	65	0.00	0	0	0.001	0	0	0				
AC331	340–343	1.769	5	0.00	0	0	0.000	0	0	0				
AC332	383–386	1.648	13	0.00	0	18	0.000	0	18	18	1000			
AC333	392–396	3.583	261	0.00	0	767	0.001	0	1342	1342		1		
AC334	403–406	2.959	430	0.23	0	173	0.001	0	363	363				
AC335	413–416	2.785	0	0.00	0	0	0.000	0	0	0				
AC348	459–464	3.025	51	0.00	8	42	0.001	0	35	35		40		
AC347	464–469	3.577	58	0.00	31	81	0.001	0	26	26		24		
AC346	469–475	3.075	132	0.00	68	193	0.001	0	0	0				
AC345	475–480	3.929	102	0.00	13	113	0.001	0	0	0				
AC344	480–485	3.720	148	0.00	190	264	0.001	53	0	53			13	1
AC343	485–491	4.472	849	0.24	85	249	0.001	12	0	12			2500	250
AC342	491–493	8.719	435	6.90	38	0	0.000	0	0	0			0	0
AC341	493–498	4.069	258	1.55	166	373	0.001	73	0	73			0	0
AC340	498–503	4.310	268	0.37	274	714	0.001	0	855	855			0	0

Diamond polymorphs include n-diamonds in carbon spherules and elongates and hexagonal and cubic found only in association with elongates.
*Embedded in carbonaceous matrix.
†Profile 2.